

Thematic Mapper Analysis of Tree Cover in Semiarid Woodlands Using a Model of Canopy Shadowing

Janet Franklin

Department of Geography, San Diego State University

Frank W. Davis

*Department of Geography and Center for Remote Sensing and Environmental Optics,
University of California, Santa Barbara*

Paul Lefebvre

Woods Hole Research Center

*The effect of variable tree canopy cover, shadows, and topography on Thematic Mapper (TM) data was examined for blue oak (*Quercus douglasii*) woodland and wooded grassland on rugged terrain in central California. Thematic Mapper data were analyzed from September 1986 (trees in leaf, grass understory senescent) and December 1984 (trees leafless, grasses emerging). Tree cover measured in 84 60 m × 60 m field plots was strongly negatively correlated with TM radiances (excluding Band 6) on both dates, and was positively correlated with the Normalized Difference Vegetation Index (NDVI) in September. TM Band 3 was most highly correlated with canopy cover. The Li–Strahler geometric–optical canopy reflectance model was used to predict the projected cover of shadow cast by the trees based on crown and illumination geometry. The spectral model was ag-*

gregated to two components; figure (tree plus shadow) and background (understory), and the pixel radiances modeled as a function of the cover of the figure. Simulated shadow cover was high at intermediate cover values, and was nonlinearly related to canopy cover. Modeled figure cover in the sample plots at the time of the satellite overpasses was more highly correlated with TM Band 3 than measured tree cover in both September (regression r^2 of 0.76 vs. 0.69) and December (r^2 of 0.59 vs. 0.53). Slope illumination explained an additional 11% of the variance in the December data. The remaining unexplained variance probably resulted from spatial variation in understory and canopy reflectances.

INTRODUCTION

Drought-deciduous woodland and wooded grassland are vegetation formations in which the herb stratum is fairly continuous, tree and shrub cover is greater than 10% and less than 60%, where fire

Address correspondence to Janet Franklin, Department of Geography, San Diego State University, San Diego, CA 92182.

Received 26 November 1990; revised 13 March 1991.

occurs, and where plant growth is closely tied to alternating wet and dry seasons (e.g., UNESCO, 1973; Walker, 1981). These formations are widespread over both temperate and tropical latitudes and are especially susceptible to climate change affecting seasonal and annual water balance, and to degradation and loss of woody cover due to human activities such as burning, grazing, and cutting (e.g., Strang, 1974; Eagleson and Segarra, 1985).

A number of studies have considered the use of optical satellite data for monitoring tree canopy extent and condition in semiarid woodlands. The presence of widely separated trees over a contrasting background of herbs and bare soil makes woodland reflectance highly sensitive to pixel resolution (e.g., Lacaze et al., 1983; Jupp et al., 1989). Reflectance is also sensitive to tree shadows, which vary as a function of tree size and spacing and the angle of incident sunlight (e.g., Pech and Davis, 1987; Jasinski, 1990; Ranson and Daughtry, 1987).

Woodland reflectance has been modeled as the sum of area-weighted contributions from different scene components, for example, sunlit tree canopy, sunlit background (ground layer) and shadows (Otterman, 1984; Li and Strahler, 1985; Jupp et al., 1986; Pech and Davis, 1987; Franklin and Strahler, 1988; Jasinski and Eagleson, 1990). In the geometric-optical approach, tree canopies are treated as three-dimensional objects casting uniform shadows on a spectrally homogeneous background or ground layer. Given specified earth-sun geometry, tree size and tree density probability distribution functions, and spectral signatures of scene components, geometric-optical models can be inverted to retrieve information about the tree layer from satellite data (Li and Strahler, 1985; Franklin and Strahler, 1988; Strahler et al., 1988). Specifying additional scene components such as relative proportions of bare soil and litter provides a more realistic model, but the added dimensionality prevents the inversion of available satellite data to estimate scene components (Jupp et al., 1986).

The development of geometric-optical canopy models has contributed greatly to our understanding of the relationship between physical and biological properties of woodlands and their spectral reflectances at different pixel sizes. Application of these models to quantify the extent and condition of the woody plant layer in woodland and wooded grassland ecosystems appears promising, but thus

far has only been attempted in areas of low relief and over a fairly narrow range of vegetation and soil conditions (e.g., Jupp et al., 1986; Franklin and Strahler, 1988). However, many semiarid woodlands occur in heterogeneous terrain that varies in topography, illumination, soil depth and mineralogy, and vegetation composition. Explicit scene modeling over such land surfaces requires accurate digital terrain data and may require separate parameter sets for different land classes, season, and image resolution. Given the difficulty of parameterizing and inverting canopy models, it is important to understand the trade-offs between increased predictive skill versus model complexity in moving from simple correlative models to more physically-based approaches.

In this paper field measurements of plant geometry and spacing are combined with geometric-optical modeling of canopy shadow to analyze blue oak (*Quercus douglasii*) woodlands and wooded grasslands in Thematic Mapper (TM) imagery from California during late summer (leaf on) and early winter (leaf off). Our objectives are to determine the contributions of tree canopy cover, canopy shadows, and topography to spatial and temporal variation in TM radiances. The effect of tree shadows on TM radiances is investigated by comparing the relationship between TM data and measured tree canopy cover with and without a shadow correction factor obtained by geometric-optical modeling.

STUDY AREA

Blue oak woodlands and wooded grasslands occupy 1.18×10^6 ha in California and are of considerable economic and ecological importance for grazing, timber production and wildlife habitat (Bolsinger, 1987). We analyzed blue oak stands in TM imagery of the Coast Ranges of San Luis Obispo County in central, coastal California (35°N, 120°E, Fig. 1). The research was part of studies in collaboration with the U.S. Forest Service on the distribution, ecology, and regeneration of blue oak in the region (Borchert et al., 1989; 1990).

Regional climate is mediterranean. Annual precipitation at lower elevations averages 527 mm, most of which falls between November and March. Elevation ranges from 520 m to 1050 m, and

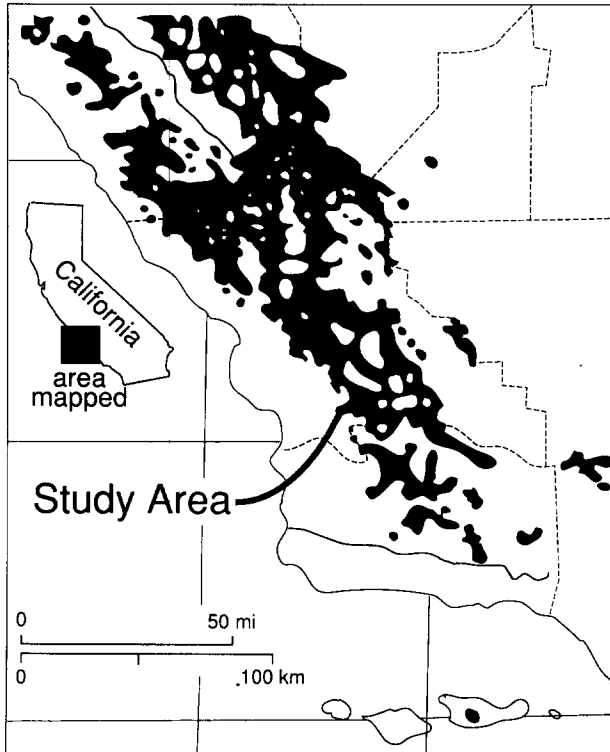


Figure 1. Study area in the Los Padres National Forest, Coast Ranges, San Luis Obispo County, California. Areas supporting blue oak woodlands are shown in black. Arrow indicates the vicinity of the study plots.

slopes average 17° [see Dubayah et al. (1989) for a quantitative analysis of regional topography]. The mean annual temperature at lower elevations is 15°C , with monthly averages ranging from 5°C to 25°C . The predominant soils are reddish-brown sandy loams derived from Tertiary sandstone and shales.

The regional vegetation is a mosaic of evergreen chaparral, annual grasslands, oak grasslands (*Quercus lobata*, *Q. douglasii*) and oak woodland (*Q. douglasii*, *Q. agrifolia*, *Pinus sabiniana*). Blue oak woodland and grassland occupy 40% of the region, with higher oak density and cover on steep north facing slopes. Most areas are grazed by cattle.

The tree layer in blue oak woodlands is open, with a well-defined overstory stratum, a sparse shrub stratum, and a dense herbaceous layer dominated by annual grasses. Griffin (1988) distinguished three different structural classes in the Central Coast Ranges, including a relatively dense woodland of small trees common on north slopes,

a more open woodland of larger trees on terraces, and a sparse oak grassland of isolated large trees on ridges and some south facing slopes. For the purposes of geometric-optical modeling, we discriminated these three types based on three canopy cover classes of 0–20%, 21–40%, and $>40\%$, respectively.

Blue oaks have small ($<15\text{ cm}^2$), sclerophyllous, deciduous leaves that are produced in April and begin senescing the late August. Leaves are distributed in compact clusters at the canopy periphery. Maximum seasonal sunlight interception by blue oak canopies ranges from 20% to 60% (Calloway, 1990). In drought years, most leaves are dropped by early October, whereas in wetter years leaf fall may continue until November (Griffin, 1988).

The herb layer in blue oak woodlands is a diverse assemblage of grasses and forbs. Total herb cover exceeds 80% in stands not excessively grazed by cattle. The annual grasses *Bromus diandrus*, *B. mollis*, and *Avena barbata* dominate most sites, but total herb cover decreases and the proportion of forb cover increases with increasing oak canopy and on more mesic north facing slopes (Borchert et al., 1990). *Avena barbata* commences growth in mid-October, attaining maximum growth rates in late March to early April and maximum standing green biomass by mid-April (Heady, 1988). Most other annual species germinate in early winter and reach highest growth rates and standing green biomass in late April and early May, respectively. The dominant annual grasses senesce by late May, although a few grasses are active through early August, and some forb species remain green throughout the summer and senesce during September (Heady, 1988).

DATA COLLECTION

Field measurements of slope angle, slope aspect, and tree basal area were collected during spring and summer 1987 in 84 $60\text{ m} \times 60\text{ m}$ plots scattered throughout a 150 km^2 study region. Plots were located subjectively by U.S. Forest Service ecologists to sample the range of stand densities (including nonwooded grassland) and terrain conditions in the study area, and were centered in stands of relatively homogeneous physical and

vegetational characteristics. Shrub cover was usually <1% and did not exceed 10% in any of the sample plots. The most frequent shrub was *Artemisia californica*, a short (<1 m), drought-deciduous shrub with a sparse canopy. We neglected the contribution of the shrub layer to canopy cover and shadows in this study.

Diameter at breast height was measured for all trees that occurred within a 0.1 acre (407 m²) circular subplot centered in the 60 m × 60 m plot. Estimates of overstory crown cover were obtained from 1:24,000 color stereo air photos acquired in September 1983. Crown cover within each plot was measured by magnifying the air photos to 1:8000 and estimating total tree canopy cover (5% cover classes) by dot count of a 10 m grid. Measured crown cover ranges from 0% to 70%.

We analyzed TM data (Path 42, Row 36) from 16 September 1986 and 14 December 1984. Oak woodlands in the September scene presented canopies that were green or in early stages of leaf senescence against a background of bright, dry soil, dry soil litter, and standing dead grasses. In contrast, oak woodlands in December consisted of leafless oaks against a background of wet soil, soil litter, and standing dead and emergent green grasses. The amount of standing herbaceous material on both dates varied with the intensity of cattle grazing. Most plots were moderately to heavily grazed, and thus supported little standing material on either date. For these plots, the major seasonal differences would be the presence of dry soil and bright soil litter in September versus wet soil, reduced soil litter, and emergent green grasses in December.

The two TM scenes were rectified and coregistered in Universal Transverse Mercator (UTM) Projection. Clear atmospheric conditions prevailed on both dates. Radiance data were corrected for atmospheric effects by dark pixel subtraction (Moik, 1980) based on near-IR reflectance from a nearby reservoir. This somewhat crude correction method was used because analyses were concerned chiefly with relative pixel brightness in single bands rather than absolute radiance or reflectance values. These corrected TM spectral brightness values will be referred to as digital numbers (DN). Median DNs in all bands except the thermal band (TM 6) were extracted for a 2 × 2 window centered on each 407 m² field plot.

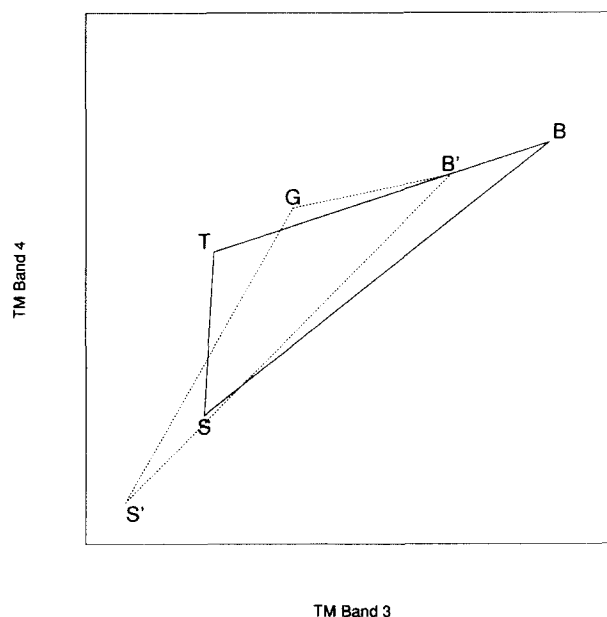
ANALYSES

Analysis of Spectral Data and Site Parameters

The spectral data for each site consisted of DNs in each TM band for September and December. Also, the Normalized Difference Vegetation Index (NDVI) (Tucker, 1979) was calculated from TM Bands 3 (.62–.69 μm) and 4 (.78–.90 μm). Huete (1988) has proposed a modification of this ratio to correct for the confounding effect of soil–vegetation interaction on NDVI. This Soil-Adjusted Vegetation Index was not tested here because tree canopies were not distributed uniformly over the soil background, consisting instead of isolated trees and intervening grassland.

The relationships among spectral data and field measurements of vegetation and topography were explored using scatterplots and correlation analysis ($n = 84$ plots). Linear least squares regression of spectral variables on oak canopy cover was carried out for the spectral variables showing the highest correlation with canopy cover. Multiple regression analyses considering tree cover, shrub cover, and

Figure 2. Schematic radiance envelope for blue oak woodland and savanna in Thematic Mapper Bands 3 and 4: The solid line describes September conditions, in which the vertices of the triangle are B (100% bare, sunlit soil), S (100% shadowed canopy or understory), and T (100% sunlit tree canopy); the broken line describes December conditions, with vertices representing B' (100% bare, sunlit soil), S' (100% shadow), and G (100% sunlit, green grasses). The diagram does not account for variable illumination due to topography (e.g., unshaded soil on different slope positions).



the cosine of local illumination angle were also conducted in an attempt to improve the prediction of spectral variation among sample plots.

Geometric–Optical Canopy Modeling

Based on the different phenologies of blue oak and understory grasses and on published reflectance data (e.g., Jasinski and Eagleson, 1990; Pech et al., 1986), we expected reflectances in TM Bands 3 and 4 (red and near infrared, respectively) to follow patterns that are shown schematically in Figure 2. In late summer, the reflectance components [sometimes termed *end members* (Smith et al., 1990)] were predicted to be bare soil (point B, high red and infrared), shadows (point S, low red and infrared), and tree canopy (point T, low red, high infrared). Position on the line from B to S is affected by increasing amounts of dry grass and shadows (both understory and overstory). Shifts in the direction of S to T are related to increasing tree cover and associated increases in green leaf area.

We expected woodland reflectance to be distinctly different in winter months, when the overstory is leafless and the understory is beginning to green up. Bare soil (B') is expected to have relatively high red and infrared reflectances, although not as high as in summer months because of higher soil moisture in December. Green understory vegetation (G) should replace trees as an end member with moderate red radiance and high infrared radiance. As cover by green grasses increases during winter months, point G should shift towards lower red radiances as bare soil is covered and as red absorption and understory shadowing increases. A spectral end member for leafless oak canopy is not shown because it presumably would fall within the winter data envelope near the shadowed soil vertex (S'). This assumption is based on reported values for red and infrared reflectance of dormant or nearly-leafless woody perennials (Graetz and Gentle, 1982; Ringrose et al., 1989; Tueller and Oleson, 1989; Franklin et al., 1991; J. Franklin, unpublished data), and on spectral modeling of sclerophyllous woodlands (Jupp et al., 1986; Pech and Davis, 1987).

In principle, the reflectance of blue oak woodland could be modeled as the area-weighted average of the projected cover of spectrally contrasting

oak crown, oak shadows, and background, with shadow area predicted from plant geometry. However, in the present study we did not have information on component spectral reflectances or their variance. We made the following simplifying assumptions: 1) the reflectance of the background (consisting of the complex understory mixture of grasses, forbs, litter, and soil) is constant over a single image, 2) there are no significant differences among the component reflectances of sunlit tree canopy, shadowed tree canopy, and shadowed understory, at least in the absorptive wavebands (Pech and Davis, 1987), and 3) component reflectances are constant over a single image. Based on these assumptions, we predicted that the variation in pixel radiance in the oak sites was attributable to differences in the relative proportions of the composite figure (sunlit tree canopy plus shadowed tree canopy and shadowed background) versus the sunlit background. For a specified sun angle and aspect, the proportion of these two components, hereafter referred to as "figure" and "background," varied as a function of tree canopy structure (e.g., density of trees, crown area, height, canopy shape) and slope orientation.

The proportion of the pixel covered by figure was estimated using the Li and Strahler (1985) canopy model. Briefly, the model assumptions are:

- (a) An oak canopy is a solid, opaque spheroid on a stick, the form of which can be parameterized from field data (Franklin and Strahler, 1988).
- (b) Tree size is lognormally distributed.
- (c) The spacing of trees is a Poisson process that can be described using field-mapped tree point pattern.
- (d) The pixel size is large enough relative to the size of individual plant canopies that a number of canopies fall within a pixel.
- (e) The spectral components are Lambertian with nonvarying reflectance signatures, and with no scattering among components.

In order to examine the magnitude of the contribution of shadow to pixel reflectance, the total cover of the figure was simulated for specified illumination conditions over the range of oak canopy cover values and topographic settings occurring in the study area. Canopy cover was subtracted from figure cover to yield shadow cover,

and shadow cover versus crown cover were plotted.

The proportion of shadowed components can be predicted from tree size (crown area) and density. However, in this study only photointerpreted canopy cover was known for each site, so an unoverlapped cover index m was calculated for each site by inverting the overlap model from Strahler et al. (1988):

$$m = nR^2 = \frac{-\ln(1-C)}{\pi}, \quad (1)$$

where n is the density, R^2 the average squared crown radius per pixel, and C photointerpreted canopy cover. The value of m from (1), related to total canopy area without overlap, is used to predict the figure cover from the geometric parameter Γ .

The parameter Γ is the area of the figure (tree crown plus shaded background) created by a spheroid of unit radius, and is a function of illumination geometry and tree shape. Plants with tall stems and narrow crowns cast more shadow per unit crown area than short, wide plants. We calculated Γ for a spheroid-on-a-stick based on three crown shape parameters; h , stem height from ground to bottom of crown, and r and b , the horizontal and vertical spheroid radii using the formula from Strahler et al. (1988). Then Γ was adjusted for slope geometry using the following formula (printed incorrectly in Strahler et al. 1988, reproduced correctly here for clarity):

$$\Gamma' = \frac{\pi + (\Gamma - \pi)\cos \alpha \cos \theta}{\cos(\theta - \beta_y)}, \quad (2)$$

where

$$\beta_y = \tan^{-1}(\tan \alpha \cos \phi),$$

α is the slope angle, and ϕ is the difference between slope and solar azimuth. If north is 0 for both slope aspect and solar direction, then

$$\phi = \text{azimuth}_{\text{slope}} - \text{azimuth}_{\text{sun}}.$$

Finally, the total figure cover C' was calculated at each site using the overlap model from Strahler et al. (1988):

$$C' = 1 - e^{-m\Gamma'}. \quad (3)$$

Correlation and regression analyses were then repeated, substituting the modeled figure cover for photointerpreted cover in each site, to see if the regression relationship improved when shadowed background was included as part of cover.

Model parameterization was based on measurements of 635 trees in the region by Harvey (1989). He demonstrated that the distributions of oak canopies in a dense woodland and a wooded grassland were not significantly different from a Poisson or random process. Tree size distributions were lognormal, with average tree height and crown diameter values shown in Table 1. Average tree height was similar in the woodland and wooded grassland sites, but crowns were narrower in the woodland stand.

Solar zenith angle and azimuth at the time of the satellite overpass were 45° and 129° , respectively, for September and 66° and 146° for December. Γ values for each date were calculated based on canopy shape measurements for wooded grassland and dense woodland sites (Table 1). A third pair of Γ values was derived by averaging for stands with intermediate canopy cover (Table 1). These Γ values were assigned to each of our 84 sites based on crown cover at the site; 0–20% cover was considered wooded grassland, 21–40% open woodland, and > 40% dense woodland. Γ

Table 1. Summary of Shape Parameters for a Spheroid on a Stick Used to Model Oak Shadowing Geometry (from Harvey, 1989)

	Canopy Shape Parameters		
	Dense Woodland	Open Woodland	Wooded Grassland
Density per ha	334	—	143
n^a	146	—	143
r (horizontal radius)	1.95	—	2.85
b (vertical radius)	2.39	—	2.38
h (stem height)	2.00	—	2.00
September Γ	7.89	7.17	6.44
December Γ	10.51	9.57	8.63

^a n is the number of trees sampled to estimate the parameters (in meters).

was adjusted for slope geometry at each site for each date using Eq. (2).

RESULTS

Correlations of Oak Cover and Topography

Blue oak canopy cover was significantly associated with topography, with highest cover values on steep, north-facing slopes (Fig. 3, Table 2). Similarly, oak cover was significantly negatively associated with solar illumination at the time of the TM overpasses, particularly in December ($r = -0.51, p < 0.01$).

Oak canopy cover was only a fair predictor of oak basal area ($r = 0.65, p < 0.01$). Basal area was also greater on steeper, north-facing slopes, but the association was not as strong as that for canopy cover ($r = 0.30, p < 0.05$). Similarly, basal area was weakly associated with solar illumination at the times of TM data acquisition.

Red-Infrared Scattergrams

Observed relationships between tree cover, red and infrared DN values were generally consistent with the conceptual model shown in Figure 2. In September, pixels from stands with less than 15% tree cover had consistently high red and infrared radiances (Fig. 4a). DN values decreased with

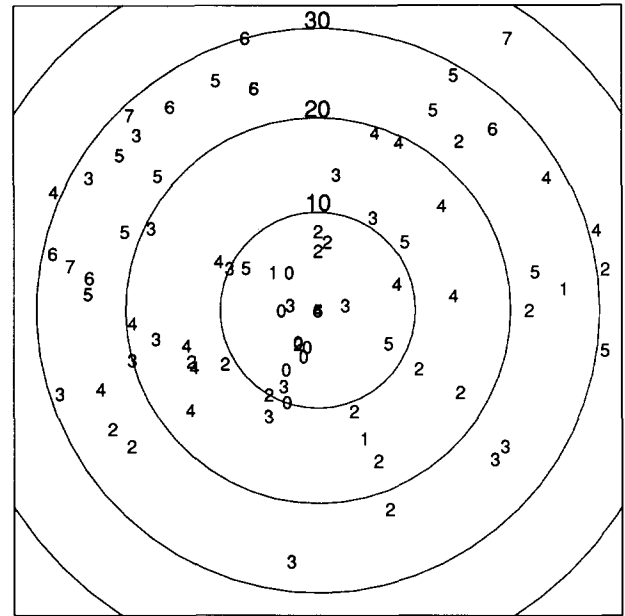


Figure 3. Polar diagram showing the distribution of oak canopy cover classes (10 percentile classes, 1 = 1–10%, 2 = 11–20%, etc.) as a function of slope angle (concentric circles indicate slopes of 10°, 20°, and 30°) and slope aspect (figure is oriented north) for 84 sample plots.

increasing tree cover, but the scatter among plots with similar cover was considerable, presumably due to other effects such as canopy condition (leaf density and senescence), illumination, and variations in understory reflectance. Grassland stands without trees exhibited considerable variation in

Figure 4. Scatter plot of DN values (after dark pixel correction) in TM Bands 3 and 4 in September (a) and December (b), for 84 sample plots in blue oak woodland and savanna. Plotted numbers indicate oak canopy cover in the plot in 10 percentile intervals (e.g., 1 = 0–10% oak cover, 2 = 11–20% oak cover, etc.).

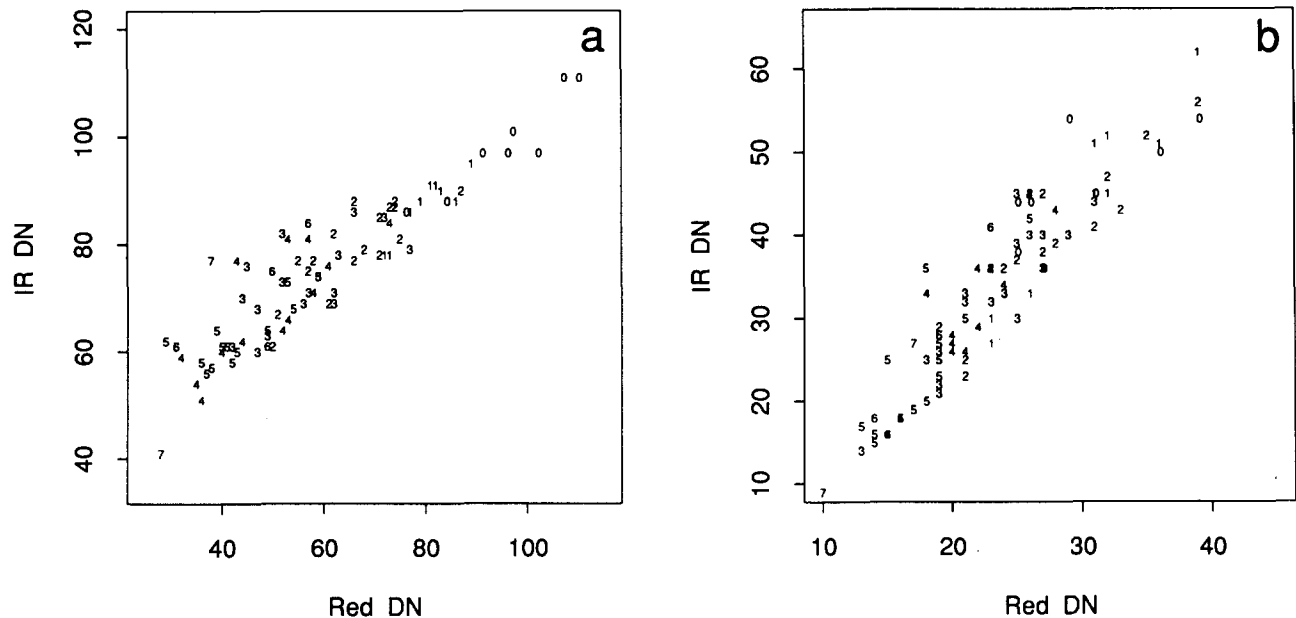


Table 2. Correlations (r) among Oak Canopy Cover, Oak Basal Area, and Topographic Variables^a

	Oak Canopy Cover	Oak Basal Area
Oak basal area	0.65**	1.00
Elevation	0.18	0.21
Northness	0.53**	0.30*
September illumination	-0.46**	-0.15
December illumination	-0.51**	-0.20

^aNorthness is defined as $\sin(\text{slope angle}) \times \cos(\text{slope aspect})$, where aspect is degrees from due north. Illumination is measured as the cosine of the angle of incident illumination on the plot at the time of TM data acquisition. Asterisks indicate significance at $p < 0.05$ (*) and $p < 0.01$ (**).

brightness (B \rightarrow S), but little variation in greenness. The variation was not related to slope orientation, and thus was likely related to variations in understory herb cover and soil reflectance.

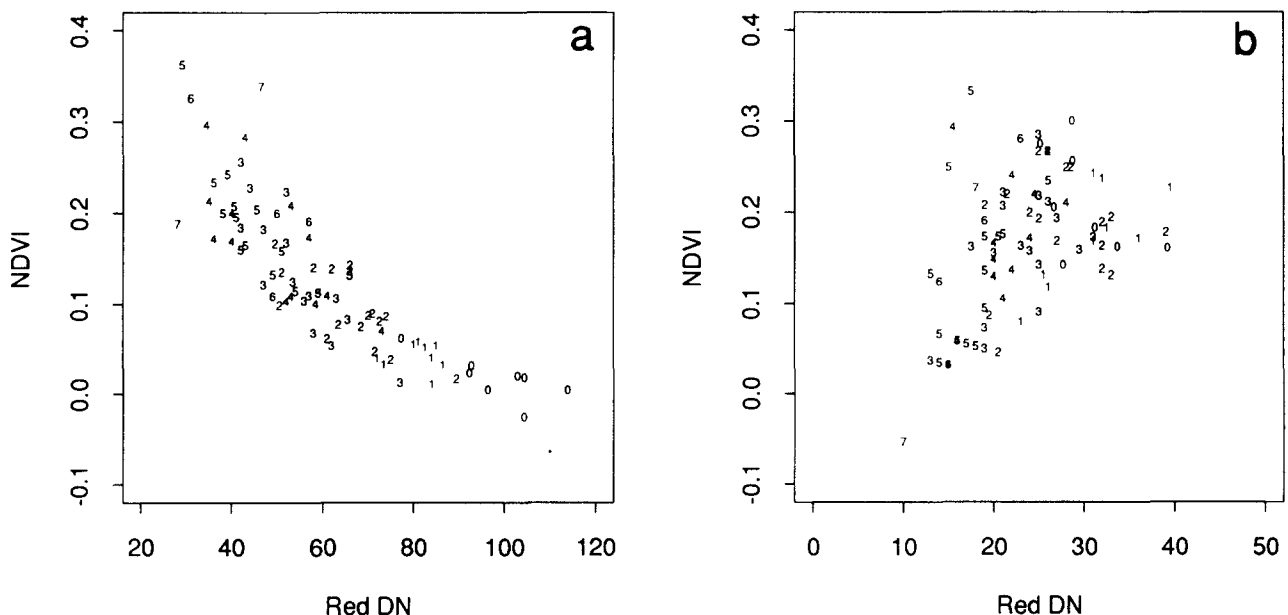
In December, stands with low tree cover exhibited greater relative variation in both red and infrared DN values (Fig. 4b). Compared to September, there was large spatial variation in illumination at this time due to the larger solar zenith angle. Based on field observations, there was also considerable spatial variation in live herbaceous biomass. Plots with high tree cover were generally dark in both red and infrared bands, and thus tended to collapse to a single "brightness" line.

Scatterplots of TM3 versus NDVI

We used scatterplots of TM3 vs. NDVI to display the pattern of "greenness" vs. "brightness" in the data (*sensu* Kauth and Thomas, 1976). In this environment, TM3 is highly correlated with multi-spectral brightness. For example, the correlation between TM3 and the first principal component axis of six TM channels (excluding TM6) is 0.98. NDVI is related although not equivalent to an additive spectral greenness index. TM4 and NDVI are only moderately correlated (e.g., $r = 0.63$ in September), so that plots of TM3 vs. TM4 display different information than TM3 vs. NDVI.

The scatterplot of NDVI versus TM3 from September bore little resemblance to that from December (Fig. 5). In September, areas with no tree cover were bright in TM3 and exhibited consistently low values of NDVI. Increasing tree cover was associated with decreasing radiances in TM3 and increasing NDVI. Given that the understory vegetation was almost entirely senescent, the large variation in NDVI within a given canopy cover class was due either to variations in canopy condition or to abiotic factors. Low rainfall during the previous winter produced unusually droughty conditions by late summer 1986, and we observed premature leaf senescence by many oaks during

Figure 5. Scatter plot of TM3 versus NDVI in September (a) and December (b) for 84 sample plots. Plotted numbers indicate oak canopy cover in the plot in 10 percentile intervals, as in Figure 4.



late August and early September. Thus there was considerable tree-to-tree variation in canopy green leaf area at the time of the TM overpass that could have increased the spectral heterogeneity of the sample stands.

In December, grasslands exhibited much greater variation in NDVI than in September, probably due to greater variation in the amount of exposed soil and variable green leaf area in the herb layer. The background was less obscured by tree canopies, which were mainly associated with decreases in TM3 and showed little association with NDVI.

Correlation of TM Data and Canopy Cover

Table 3 summarizes the correlations of oak canopy cover with the different TM bands and with NDVI. TM3 was most highly negatively correlated with canopy cover in September, although the correlation coefficients were almost as high for the other visible and middle infrared spectral bands. Image brightness was also negatively correlated with oak canopy cover in December, although correlations were significantly lower. NDVI was positively correlated with oak canopy cover in September when oaks were in leaf and the understory was senescent, and weakly negatively correlated with oak cover in December when oaks were leafless and the understory was greening up. Again, oak basal area was less strongly correlated with TM band radiances, with r ranging from -0.55 to -0.38 in September and December, respectively.

Figures 6a and 7a show the regressions of red DN against oak canopy cover on each date. Although the variation in background reflectance was evident from the range of spectral values for sites with zero percent oak canopy cover on both dates, the scatter was much greater for all canopy cover values in December. As noted previously, this is likely the result of background heterogeneity, although registration errors may also have contributed some noise. Even in September, there was a lot of variation in radiance for sites with intermediate to high canopy cover. Low precision and error in measuring oak canopy cover is another possible source of model error. However, a sizeable fraction (23–26%) of the remaining variance could be attributed to differential effects of canopy shadowing as a function of tree cover and topographic position, as demonstrated below.

Canopy Shadow Modeling

Simulated Shadows

The predicted cover of shadowed background as a function of tree canopy cover, angle of incident radiation and Γ is shown in Figure 8. The Γ values of 7.0 and 10.5 correspond to typical September and December values for our study sites, the latter casting more shadow per unit canopy area because of the lower sun angle. These values could also represent shorter, wider and taller, narrower trees under uniform illumination conditions. The values of $\cos \theta$ that are shown also represent the range of conditions found in the study sites, although for steep north-facing sites in the December image $\cos \theta$ approaches zero and shadow cover approaches the complement of canopy cover. As canopy cover increases, shadow cover first increases, and then decreases at higher cover values due to overlap. The contribution of shadow to the area of the figure is most pronounced on slopes facing away from the sun (those with low values of $\cos \theta$).

The modeled results are similar to theoretical and empirical results obtained by Jasinski (1990) for juniper woodland in the southwestern United States and by Pech and Davis (1987) for *Acacia* and eucalypt woodlands in Australia. Measurements by Pech and Davis (1987) show the extent of variability of these cover fractions measured in the field. Based on Figure 8, one would expect

Table 3. Correlations (r) of Spectral Data and Oak Canopy Cover, and Canopy Cover plus Modeled Shadow Cover, for September and December TM Imagery^a

	Oak Canopy	Oak Canopy plus Shadow
	<i>September</i>	
TM1	-0.79	-0.84
TM2	-0.81	-0.84
TM3	-0.83	-0.87
TM4	-0.76	-0.83
TM5	-0.82	-0.84
TM7	-0.79	-0.81
NDVI	0.73	0.69
	<i>December</i>	
TM1	-0.77	-0.80
TM2	-0.72	-0.78
TM3	-0.73	-0.77
TM4	-0.67	-0.76
TM5	-0.73	-0.78
TM7	-0.74	-0.78
NDVI	-0.28	-0.37

^aAll correlations are significant at $p < 0.01$.

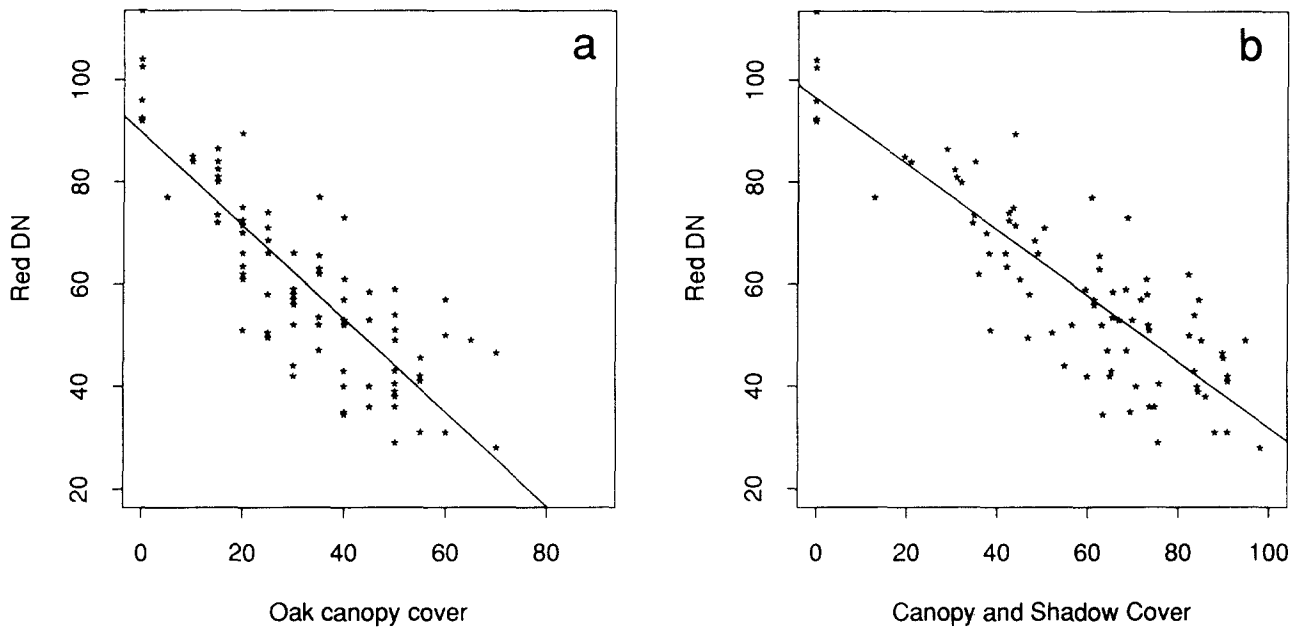


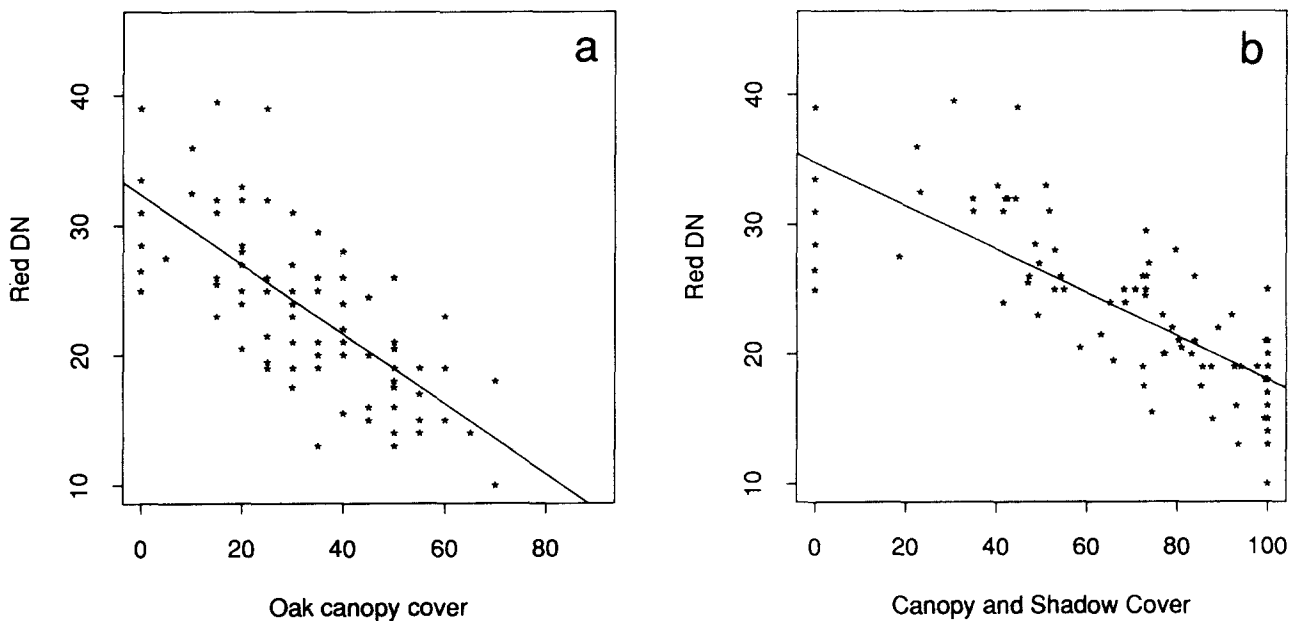
Figure 6. Regression of September TM3 DN against photointerpreted oak canopy cover (a) and canopy cover plus modeled shadow cover (b). The equation for the regression line in Figure 6a is: $Y = 89 - 0.19X$; $r^2 = 0.69$; $p < 0.01$. The equation for the regression line in Figure 6b is: $Y = 97 - 0.65X$; $r^2 = 0.75$; $p < 0.01$.

shadows to contribute 2–40% cover over the range of canopy cover and illumination conditions found in the study sites on both image dates.

Modeled Tree Cover plus Shadow for Sample Plots
When the total cover of the figure including

shadow, calculated from the geometric model [Eq. (3)], was substituted for photointerpreted crown cover in the correlation and regression analysis, correlations between band radiance and cover increased slightly for all bands (except NDVI) in September and December (Table 3). The regres-

Figure 7. Regression of December TM3 DN against photointerpreted oak canopy cover (a) and canopy cover plus modeled shadow cover (b). The equation for the regression line in Figure 7a is: $Y = 32 - 0.27X$; $r^2 = 0.53$; $p < 0.01$. The equation for the regression line in Figure 7b is: $Y = 35 - 0.17X$; $r^2 = 0.59$; $p < 0.01$.



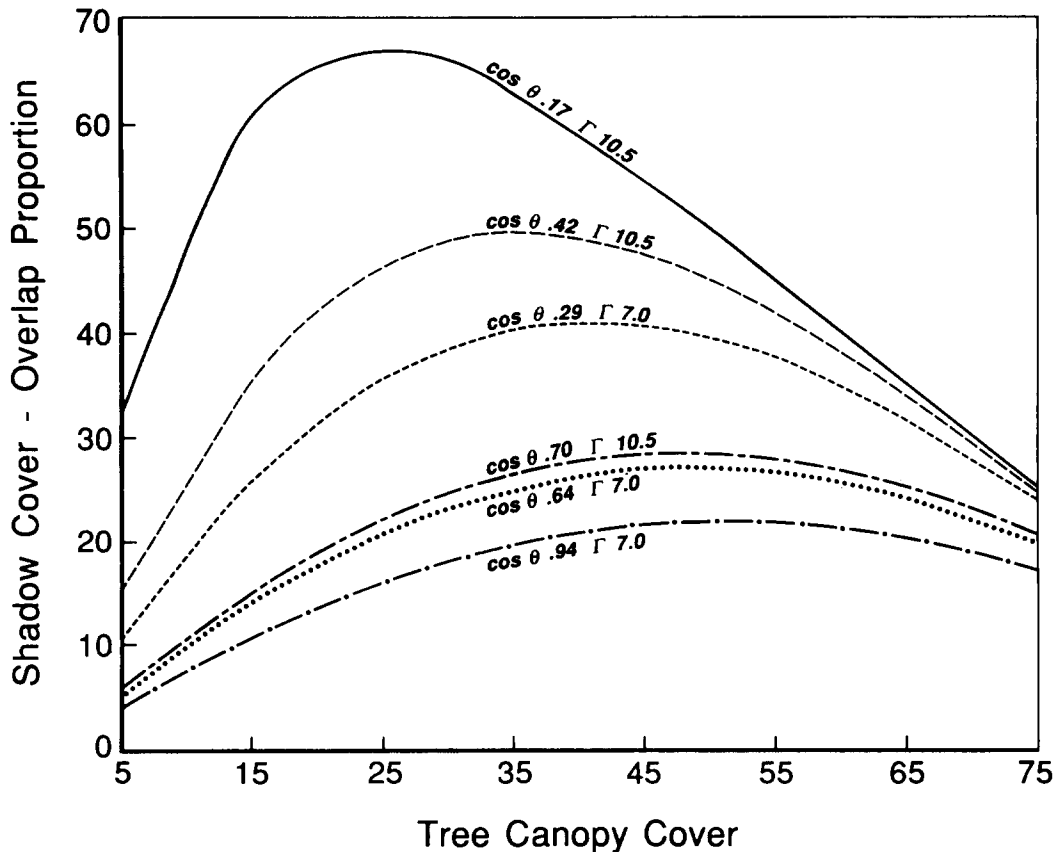


Figure 8. Oak canopy cover versus modeled shadow cover for different combinations of Γ (10.5, 7.0) and cosine (illumination angle) (0.17, 0.42, 0.7, 0.29, 0.64, 0.94) (see text for explanation of Γ and for model calculations).

sion r^2 between TM3 and oak cover improved from 0.69 to 0.76 for September and from 0.53 to 0.59 in December. Of course, modeled shadow did not affect the sites with no tree cover, and many points falling far from the regression line remained outliers after the shadow modeling. The model for December predicted 100% figure cover for many sites on north-facing slopes; this assumes that the crown area projected onto the background is entirely shadow. In fact, the amount of background covered by the leafless crown and its shadow would be less than 100% and would probably vary among sites. For leafless trees, the projected canopy cover is actually a small fraction of the crown area, and crown reflectance is a function of both the tree canopy and background signatures. (Canopy translucence could be approximated in the four-component Li-Strahler model, but that would require information on the component signatures.)

Residuals from the regression analysis of September TM3 and figure cover were not correlated with illumination ($r^2 < 0.01$), nor with shrub cover as visually estimated in the field ($r^2 = 0.05$). In December, however, residuals were significantly correlated with slope illumination ($r^2 = 0.15$, $p < 0.01$). Thus, multiple regression of December TM3 on modeled figure and the cosine of incident solar radiation provided a better fit to the data (multiple $r^2 = 0.70$, $p < 0.001$) than that based only on figure cover.

SUMMARY AND DISCUSSION

Satellite monitoring of tree canopy cover in California's blue oak woodlands is feasible using simple correlative methods, even in relatively heterogeneous terrain with variable canopy and ground

layer conditions. Tree cover is highly correlated with radiance in all TM bands in summer and winter imagery, without any compensation for varying illumination on sloping terrain, canopy shadowing or background variability, and with only minimal atmospheric correction. This is presumably because of the high spectral contrast between tree canopies and ground layer in summer and early winter, as well as the high correlation of oak cover with topography and scene illumination. Unfortunately, tree basal area in oak woodlands, which is a better predictor of biomass than canopy cover, is not as highly correlated with canopy cover or with satellite radiances.

Including a simple geometric model of canopy shadowing on sloping terrain significantly improves the relationship between oak cover and radiance. In this study, variations in oak canopy cover accounted for 69% of the variance in TM3 DN values in September and 53% in December. In comparison, oak canopy and modeled shadows explained 76% of the variance in DN values in September and 59% in December. Finally, accounting for oak cover, shadows and illumination explained 70% of the variance in December TM3 DN levels.

The remaining 24–30% unexplained variance in TM data probably has several sources, including unknown changes in tree cover between 1983 and 1986 (which we presume are very small, based on observations of permanent study plots in the region), errors in estimating tree cover in the sample plots, variations in canopy and background reflectances, and imperfect specification of the geometric–optical model. In particular, it was certainly an oversimplification to regard the background and the composite figure each as having a uniform spectral signature.

Given their structural and spectral simplicity, we expect that comparable results will be obtained for other semiarid woodlands and wooded grasslands. Whether invertible models can be applied successfully to estimate tree cover in such environments will depend on other factors not considered in our analysis, especially the relationship between sensor resolution, tree size distribution, and the characteristic scales of vegetation pattern. In our study area, blue oak crowns are large enough that there is considerable within-stand spectral variability at 30 m TM resolution, as pixels tend to fall on or between crowns (Wood-

cock and Strahler, 1987; Jasinski and Eagleson, 1990). At lower spatial resolution, there is less within-stand spectral variation (e.g., Jupp et al., 1989), but an increased frequency of mixed pixels due to the small extent of individual stands, which tend to occur in a fine mosaic with other types such as evergreen and deciduous shrublands. The 30-m resolution of TM may be the optimal compromise for estimating oak cover in this particular vegetation mosaic, but the small size of the stands makes it difficult to use pixel variance to invert the Li–Strahler model and derive tree size and density information.

The distinctive phenology of mediterranean-climate woodlands makes their spectral dynamics somewhat different from tropical woodlands and savannas. The late summer scene is composed of dry grass, soil, litter, and crowns that are not dominated by green leaf material (e.g., low infrared reflectance) as in Jupp et al. (1986) and Walker et al. (1986). The red–infrared scattergram for late summer is reminiscent of the data envelopes modeled by Pech et al. (1986) for a mixture of grass and woody vegetation (in their case shrubs) and including canopy shadows, at low sun angles. However, they modeled a scene that included green grass and green shrubs. Our red–infrared data envelope collapses because the tree canopy is not green, rather than because of the shadowing of green grass by tree canopies. The relationship between cover and the red–infrared scattergram is similar, in principal, to that modeled by Jasinski and Eagleson (1989;1990), but again our scattergram looks different because vegetation in the scene is not very green. The shape of the December red–infrared scattergram can be explained in terms of the patchy distribution of the green herb understory, partly covered by dark leafless canopies and shaded slopes. The correlation of oak cover with north-facing slopes means that the points on the scattergram converge at the low end, because both trees and shadows are dark in that season.

From a practical perspective, there is a trade-off between model complexity and applicability in using geometric–optical modeling for woodland inventory. For the purpose of inventorying blue oak resources, a simple relationship between red reflectance and cover may be adequate, provided that imagery is acquired when there is high spectral contrast between oak canopy and background,

and when the background reflectance is relatively uniform (e.g., late summer). Because almost any area will have large background reflectance variability it may be possible and necessary to fit a family of regression models. In rugged terrain, presuming that accurate digital elevation data are available, the more complex, physically-based geometric-optical model should provide higher accuracy and more detailed biophysical information on the amount and distribution of tree cover.

This research was supported by California Space Institute Grant CS-59-88. We thank M. Borchert of the Los Padres National Forest and L. E. Harvey, Queen's University, Ontario for providing field data on oak size distributions and plot basal area. We are grateful to M. Jasinski, NASA Goddard Space Flight Center, A. Strahler, Boston University, and R. Dubayah, University of Maryland, for helpful discussions and comments on the draft manuscript, and to two anonymous reviewers for additional comments and improvements.

REFERENCES

- Bolsinger, C. L. (1987), Major findings of a statewide hardwood inventory, in *Proceedings of the Symposium on Multiple-use Management of California's Hardwood Resources* (T. R. Plumb and N. H. Pillsbury, Eds.), United States Forest Service Pacific Southwest Forest and Range Experiment Station, pp. 291–297.
- Borchert, M., Davis, F. W., Michaelsen, J. C., and Oyler, L. D. (1989), Interactions of factors affecting seedling recruitment of blue oak (*Quercus douglasii*) in California, *Ecology* 70:389–404.
- Borchert, M., Davis, F. W., and Allen-Diaz, B. (1990), Environmental relationships of herbs in blue oak (*Quercus douglasii*) woodlands of central coastal California, *Madroño*, forthcoming.
- Calloway, R. (1990), Variable effects of *Quercus douglasii* on neighbors: from facilitation to interference, Ph.D. dissertation, University of California, Santa Barbara.
- Dubayah, R. O., Dozier, J., and Davis, F. W. (1989), The distribution of clear-sky radiation over varying terrain, *Proc. IGARSS' 89*:885–888.
- Eagleson, P. S., and Segarra, R. I. (1985), Water-limited equilibrium of savanna vegetation systems, *Water Resour. Res.* 21:1483–1493.
- Franklin, J., and Strahler, A. H. (1988), Invertible canopy reflectance modeling of vegetation structure in semiarid savanna, *IEEE Trans. Geosci. Remote Sens.* GE-26:809–825.
- Franklin, J., Prince, S. D., Strahler, A. H., Hanan, N., and Simonett, D. S. (1991), Reflectance and transmission properties of West African savanna trees from ground radiometer measurements, *Int. J. Remote Sens.*, forthcoming.
- Graetz, R. D., and Gentle, M. R. (1982), The relationships between reflectance in the Landsat wavebands and the composition of an Australian semi-arid shrub rangeland, *Photogram. Eng. Remote Sens.* 48:1721–1730.
- Griffin, J. R. (1988), Oak woodland, in *Terrestrial Vegetation of California* (M. G. Barbour and J. Major, Eds.), Wiley, New York, pp. 383–416.
- Harvey, L. E. (1989), Spatial and temporal dynamics of a blue oak woodland, Ph.D. dissertation, Department of Geography University of California, Santa Barbara, 170 pp.
- Heady, H. F. (1988), Valley Grassland, in *Terrestrial Vegetation of California* (J. Major, Ed.), Wiley, New York, pp. 491–514.
- Huete, A. R. (1988), A Soil-Adjusted Vegetation Index (SAVI), *Remote Sens. Environ.* 25:295–309.
- Jasinski, M. F. (1990), Functional relation among subpixel canopy cover, ground shadow, and illuminated ground at large sampling scales, in *Remote Sensing of the Biosphere*, Society of Photo Optical Instrumentation Engineers, Bellingham, WA.
- Jasinski, M. F., and Eagleson, P. S. (1989), The structure of red-infrared scattergrams of semivegetated landscapes, *IEEE Trans. Geosci. Remote Sens.* GE-27:441–451.
- Jasinski, M. F., and Eagleson, P. S. (1990), Estimation of subpixel vegetation cover using red-infrared scattergrams, *IEEE Trans. Geosci. Remote Sens.* GE-28:253–267.
- Jupp, D. L. B., Walker, J., and Penridge, L. K. (1986), Interpretation of vegetation structure in Landsat MSS imagery: a case study in disturbed semi-arid Eucalypt woodlands. Part 2. Model-based analysis, *J. Environ. Manage.* 23:35–57.
- Jupp, D. L. B., Strahler, A. H., and Woodcock, C. E. (1989), Autocorrelation and regularization in digital images II. Simple image models, *IEEE Trans. Geosci. Remote Sens.* 27:247–256.
- Kauth, R. J., and Thomas, G. S. (1976), The tasseled cap—a graphic description of the spectral-temporal development of crops as seen by Landsat, in *Proc. Symp. on Machine Processing of Remotely Sensed Data*, Purdue Univ., West Lafayette, IN, pp. 41–51.
- Lacaze, B., Debussche, G., and Jardel, J. (1983), Spatial variability of mediterranean woodlands as deduced from Landsat and ground measurements, *Proc. IGARSS' 83*:4.1–4.5.
- Li, X., and Strahler, A. H. (1985), Geometric-optical modeling of a conifer forest canopy, *IEEE Trans. Geosci. Remote Sens.* GE-23:705–721.
- Moik, J. G. (1980), *Digital Processing of Remotely Sensed Images*, NASA, Washington, DC.
- Otterman, J. (1984), Albedo of a forest modeled as a plane with dense vertical protrusions, *J. Climate Appl. Meteorol.* 22:297–307.
- Pech, R. P., and Davis, A. W. (1987), Reflectance modeling of semiarid woodlands, *Remote Sens. Environ.* 23:365–377.

- Pech, R. P., Graetz, R. D., and Davis, A. W. (1986), Reflectance modelling and the derivation of vegetation indices for an Australian semi-arid shrubland, *Int. J. Remote Sens.* 7:389–403.
- Ranson, J. K., and Daughtry, C. S. (1987), Scene shadow effects on multispectral response, *IEEE Trans. Geosci. Remote Sens.* GE-25:502–509.
- Ringrose, S., Matheson, W., Mogotsi, B., and Tempest, F. (1989), The darkening effect in drought affected savanna woodland environments relative to soil reflectance and SPOT wavebands, *Remote Sens. Environ.* 30:1–19.
- Smith, M. O., Ustin, S. L., Adams, J. B., and Gillespie, A. R. (1990), Vegetation in deserts: I. A regional measure of abundance from multispectral images, *Remote Sens. Environ.* 31:1–26.
- Strahler, A. H., Wu, Y., and Franklin, J. (1988), Remote estimation of tree size and density from satellite imagery by inversion of a geometric–optical canopy model, in *Proceedings of the 22nd International Symposium on Remote Sensing of Environment*, Abidjan, Côte d'Ivoire, Environmental Research Institute of Michigan, Ann Arbor, MI, pp. 337–348.
- Strang, R. M. (1974), Some man-made changes in successional trends on the Rhodesian highveld, *J. Appl. Ecol.* 11:249–263.
- Tucker, C. J. (1979), Red and photographic infrared linear combinations for monitoring vegetation, *Remote Sens. Environ.* 8:127–150.
- Tueller, P. T., and Oleson, S. G. (1989), Diurnal radiance and shadow fluctuations in a cold desert shrub plant community, *Remote Sens. Environ.* 29:1–13.
- UNESCO (1973), *International Classification and Mapping of Vegetation*, United Nations Educational, Scientific and Cultural Organization, Paris, 93 pp.
- Walker, B. H. (1981), Is succession a viable concept in savannah ecosystems?, in *Forest Succession: Concepts and Applications* (D. C. West et al., Eds.), Springer-Verlag, New York, pp. 431–447.
- Walker, J., Jupp, D. L. B., Penridge, L. K., and Tian, G. (1986), Interpretation of vegetation structure in Landsat MSS imagery: a case study in disturbed semi-arid eucalypt woodlots. Part 1. Field data analysis, *J. Environ. Manage.* 23:19–23.
- Woodcock, C. E., and Strahler, A. H. (1987), The factor of scale in remote sensing, *Remote Sens. Environ.* 21:311–332.